J. Am. Ceram. Soc., 95 [11] 3597–3604 (2012)
DOI: 10.1111/j.1551-2916.2012.05371.x

journal

The Electronic Structures, Born Effective Charges, and Interatomic Force Constants in $BaMO_3$ (M = Ti, Zr, Hf, Sn): A Comparative First-Principles Study

L. Xie[‡§] and J. Zhu[‡,§,†]

[‡]Beijing National Center for Electron Microscopy, Tsinghua University, Beijing 100084, China

[§]Department of Materials Science and Engineering, The State Key Laboratory of New Ceramics and Fine Processing, Laboratory of Advanced Materials, Tsinghua University, Beijing 100084, China

The electronic structures, Born effective charges (BEC), and interatomic force constants of $BaMO_3$ (M = Ti, Zr, Hf, Sn) in the cubic perovskite structure are computed using first-principles density functional theory. Comparison with the Maximally-localized Wannier function description of the electronic structures for $BaTiO_3$ shows that the change of a single constituent (Ti to Zr, Hf, and Sn) has pronounce effects on the orbital hybridizations with the oxygen, with significant implications for the nature of the BEC anomalous of the compounds. Examination of the real-space interatomic force constants shows that the key interatomic interactions are strongly dependent on the constituent's dynamical effective charge and the very delicate compensation between the short-range interactions and long-range dipole–dipole interactions gives rise to the ferroelectric structural instabilities.

I. Introduction

Materials with ferroelectric properties have long been intensively researched for their wide variety of applications, such as transducers, actuators, capacitors, and memories.[1,2] Among the most investigated ferroelectric materials, the perovskite ABO_3 family is of particular interest for their structure simplicity and superior performance. Most ferroelectric oxides in the perovskite structure have a d^0 transition metal at the B-site, and the interaction between d states of the B-site atom with p states of oxygen is known to be crucial to their properties.[3] One most representative material is the ferroelectric $BaTiO_3$. However, many d^0 perovskites, such as $BaZrO_3$ and $BaHfO_3$, which hold promise as high-k dielectric materials,[4] are known to remain the highly stabilized cubic symmetry down to liquid helium temperature. In addition to the d^0 transition metals, the B-site atom can also be chosen as those whose nominal ionic charge is +4. One such example is $BaSnO_3$, of which the tin atom is of d^{10} electronic structure and this material also remains cubic down to low temperature. These examples indicate the very complex and delicate nature of the material's electronic structure and its properties. Therefore, understanding how the electronic structure of the B-site atom and its interaction with oxygen give rise to the ferroelectric properties is of fundamental interest and will also help in designing materials with better performance.

Dielectric and ferroelectric properties are intimately associated with the electronic polarization of insulators. In the framework of modern theory of polarization,[5,6] the polarization is related to the flow of electronic charge induced due to small displacements of atoms. The strength of the charge transfer with respect to the displacements of atoms is also known as Born effective charge (BEC). In ferroelectric materials, the BEC associated with an atom is usually much larger than its nominal charge and the anomalously large effective charge is an indicator of the ferroelectric structural instabilities.[7,8] For example, the theoretical BEC of Ti in $BaTiO_3$ is +7.52, which is almost twice larger than its nominal value (+4). Recent analysis of $BaTiO_3$ based on real-space interatomic force constant (IFC)[9] has highlighted the important role played by the anomalous effective charge in giving rise to the destabilizing long-range dipolar field and the instable soft polar phonon modes. However, a systematic investigation of various B-site cations' electronic structures, BECs, and their relation to the ferroelectric instabilities is still lacking.

In this study, we present a comparative study of the electronic structure, BEC, and real-space IFC of four different cubic perovskites $BaTiO_3$, $BaZrO_3$, $BaHfO_3$, and $BaSnO_3$, computed from first-principles density functional theory (DFT) calculations using the Maximally-localized Wannier function (MLWF) and frozen phonon method as described in Section II. These compounds have been chosen both because of their scientific and technological importance, and because they allow us to investigate the effects on the electronic structure and IFC of substituting one cation, whereas other atoms remain unchanged. As we will see in Section III, the substitutions of Zr and Hf lead to a slight modification of the electronic structure and a decrease of their BECs. The substitution of Sn gives rise to very pronounced differences in the electronic structure, where its d-state electrons do not hybridize with oxygen $2p$ orbitals, and its effective charge is almost identical to its nominal value. The trends in cation–cation and cation–oxygen interactions are analyzed in terms of IFC and associated with the B-site atoms' dynamical charge transfer. There, we will see that the driving mechanism of ferroelectric can be mainly attributed to the dynamic charge transfer between the B-site atom and oxygen, and the corresponding destabilizing dipole–dipole interactions against stable short-range interactions among the four compounds.

II. Methods

The calculations of BECs and IFC reported herein were carried out using VASP software package[10] using the plane wave basis and PAW scheme[11] with the exchange-correlation potential of Perdew–Zunger parameterization.[12] The 5s, 5p of Ba, 3s, 3p of Ti, 4s, 4p of Zr, 5s, 5p of Hf, and 4d of Sn are included in the valence as semi-core states. In our calculation, the experiment lattice parameters of $BaTiO_3$ (~4.00 Å), $BaZrO_3$ (~4.192 Å), $BaHfO_3$ (~4.171 Å), and $BaSnO_3$ (~4.116 Å) are used. An energy cutoff of 600 eV of the plane-wave basis and a sampling of the Brillouin zone with a

W.-Y. Ching—contributing editor

Manuscript No. 31389. Received April 26, 2012; approved June 20, 2012.
†Author to whom correspondence should be addressed. e-mail: jzhu@mail.tsinghua.edu.cn

$9 \times 9 \times 9$ Monkhorst–Pack mesh[13] is used. The BEC and optical dielectric constant is calculated with the density functional perturbation theory (DFPT), following Refs.14 and 15. The IFC was obtained using the frozen phonon approach with a $3 \times 3 \times 3$ supercell and a $3 \times 3 \times 3$ Monkhorst–Pack mesh.[13]

The MLWFs were constructed using the full-potential linearized augmented plane wave method as implemented in the FLEUR code.[16,17] For Ba and O, muffin-tin radii of 2.8 and 1.5 a.u. were used. For B-site atoms, Ti, Zr, Hf, and Sn, their muffin-tin radii were 2.1, 2.5, 2.45, and 2.55 a.u., respectively. The exchange-correlation functional was evaluated within the local density approximation using the Perdew–Zunger parametrization[12] and the plane-wave cutoff was chosen to be 4.8 a.u.$^{-1}$. The MLWFs were constructed using a $4 \times 4 \times 4$ uniform mesh of k-points using the post-processing software Wannier90.[18]

(1) Maximally-Localized Wannier Functions

The electronic structure of periodic materials are typically described by a set of Bloch states $\psi_{n\mathbf{k}}$, where the states are characterized by the band index n and the wave vector $\mathbf{k}$. An alternative representation of the electronic structure can be given in terms of MLWFs, which are a set of localized functions in the real space. The MLWF centered on a lattice site $\mathbf{R}$, $W_{n\mathbf{R}}(\mathbf{r})$, is obtained using Fourier transform of the Bloch functions of occupied bands as:

$$W_{n\mathbf{R}}(\mathbf{r}) = \frac{\Omega_0}{(2\pi)^3} \int_{\mathrm{BZ}} \left[\sum_{\mathrm{m}} U_{mn}^{(\mathbf{k})} \psi_{m\mathbf{k}}(\mathbf{r}) \right] e^{-i\mathbf{k}\cdot\mathbf{r}} \mathrm{d}\mathbf{k} \tag{1}$$

where Ω_0 is the unit cell volume, the integral is over the Brillouin zone (BZ) and $U_{mn}^{(\mathbf{k})}$ is a unitary matrix that mixes the Bloch state at each wave vector $\mathbf{k}$. At any wave vector $\mathbf{k}$, $U_{mn}^{(\mathbf{k})}$ is nonunique, as any unitary transformation is a valid description of the electronic structure and different choices will lead to MLWF with varying spatial localizations. As a result, MLWFs are also not uniquely defined. Nevertheless, several heuristic choices of the unitary transformation have been developed, which are known to yield maximally localized sets of MLWFs.[18,19]

In ionic-covalent mixed crystals, the MLWFs are typically centered on atom sites and resemble localized atomic orbitals despite the underlying crystal potential. Their delocalized distribution to the neighboring atoms and the overlap between the atomic orbitals indicate the degree of charge transfer and covalency. For the $BaMO_3$ materials studied herein, the MLWFs can be separated into several groups by the gaps between the occupied bands. For instance, the band groups of $BaTiO_3$, from the lowest occupied valence band to the highest, correspond to the Ti 3*s*, Ti 3*p*, Ba 5*s*, O 2*s*, Ba 5*p*, and O 2*p* levels, respectively. Among these bands, the O 2*p* bands in the vicinity of Fermi surface play a most important role on the charge transfer and hybridization between the oxygen and B-site atoms. We initially consider the highest occupied bands by nine O 2*p* atomic orbitals centered on three O sites and perform the minimization of the maximally localized MLWFs.

(2) Born Effective Charge

The BEC describes the change in macroscopic polarization that is induced by the displacement of a given ion. The BEC of an atom is a tensor, whose elements $Z^*_{i,\alpha\beta}$ are defined as the change of polarization P_β per unit cell in β direction to the displacement of atom i in α direction:

$$Z^*_{i,\alpha\beta} = \frac{\partial P_\beta}{\partial u_{i,\alpha}} \qquad \text{P including ionic part (rigid shift)} \tag{2}$$

where $u_{i,\alpha}$ is the α component of the displacement of atom i.

In the framework of modern theory of polarization,[5,6] the BEC associated with a dipole induced by the displacement of atom i is given by:

$$Z^*_{i,\alpha\beta} = Z_i^{\mathrm{ion}} \delta_{\alpha\beta} + \frac{\Omega_0}{|e|} \frac{\partial P_{\mathrm{e},\beta}}{\partial u_{i,\alpha}} \tag{3}$$

where $\delta_{\alpha\beta}$ is the Kronecker's delta, Z_i^{ion} is the ionic charge (=number of valence electrons of the given atom) and $P_{\mathrm{e},\beta}$ is the electronic polarization of valence electrons in β direction. The ionic charge term $Z_i^{\mathrm{ion}}\delta_{\alpha\beta}$ describes the rigid shift of the charges with respect to the ion's displacement, while the electronic response $\frac{\partial P_{\mathrm{e},\beta}}{\partial u_{i,\alpha}}$ is related with the dynamic charge transfer of valence electrons. Using the MLWFs' descriptions of electronic structure, the electronic polarization $\mathbf{P}_\mathrm{e}$ associated with the valence electrons can be written as the sum of individual MLWFs:

$$\mathbf{P}_\mathrm{e} = -\frac{f|e|}{\Omega_0} \sum_n \langle W_{n0}(\mathbf{r}) | \mathbf{r} | W_{n0}(\mathbf{r}) \rangle \tag{4}$$

where f and e is the occupation number of the n-th band and the electronic charge, respectively. The expectation value of position operator $\langle W_{n0}(\mathbf{r}) | \mathbf{r} | W_{n0}(\mathbf{r}) \rangle$ is also called the Wannier center. Combining Eqs. (3) and (4), the BEC can then be written as:

$$Z^*_{i,\alpha\beta} = Z_i^{\mathrm{ion}} \delta_{\alpha\beta} - f \sum_n \frac{\partial \langle W_{n0}(\mathbf{r}) | \mathbf{r} | W_{n0}(\mathbf{r}) \rangle_\beta}{\partial u_{i,\alpha}} \tag{5}$$

Equation (5) associates the MLWFs and the BEC in a straightforward way, where the BEC can be decomposed into individual contributions from the occupied bands and the MLWFs.

(3) Interatomic Force Constants

The interatomic force constants are generated in the construction of the phonon dispersion relations. The IFC matrix $\Phi_{\kappa\alpha,\kappa'\beta}(i,j)$ relates the force $F_{\kappa\alpha}(i)$ felt by atom κ in cell i with respect to the displacement $\Delta u_{\kappa'\beta}(j)$ of atom κ' in cell j and is defined as:

$$F_{\kappa\alpha}(i) = -\Phi_{\kappa\alpha,\kappa'\beta}(i,j) \Delta u_{\kappa'\beta}(j) \tag{6}$$

For insulating materials, although somewhat arbitrary, the total IFC $\Phi_{\kappa\alpha,\kappa'\beta}(i,j)$ can be decomposed into a long-range dipole–dipole (DD) interaction part $\Phi^{\mathrm{DD}}_{\kappa\alpha,\kappa'\beta}(i,j)$ and a short-range (SR) part $\Phi^{\mathrm{SR}}_{\kappa\alpha,\kappa'\beta}(i,j)$[20,21]:

$$\Phi_{\kappa\alpha,\kappa'\beta}(i,j) = \Phi^{\mathrm{DD}}_{\kappa\alpha,\kappa'\beta}(i,j) + \Phi^{\mathrm{SR}}_{\kappa\alpha,\kappa'\beta}(i,j) \tag{7}$$

Such decomposition is very useful in the analysis of the microscopic origin of the ferroelectric instability and the competition between the long-range and short-range interactions among different compounds.

The long-range dipole–dipole interaction term decays as a function of the atomic distance r ($\alpha\ r^{-3}$) and can be analytically written as a function of optical dielectric constant tensor ε_∞ and BECs[20]:

$$\Phi^{\mathrm{DD}}_{\kappa\alpha,\kappa'\beta}(i,j) = \frac{1}{4\pi\varepsilon_0} (\det \varepsilon_\infty)^{-\frac{1}{2}} \sum_{\alpha'\beta'} Z^*_{\kappa,\alpha\alpha'} Z^*_{\kappa',\beta\beta'} \times \left[\frac{\left(\varepsilon_\infty^{-1}\right)_{\alpha'\beta'}}{D^3} - 3\frac{\Delta_{\alpha'\beta'}}{D^5} \right] \tag{8}$$

where $Z^*_{\kappa,\alpha\alpha'}$ is the BEC tensor of atom κ, $\Delta_\alpha = \sum \left(\varepsilon_\infty^{-1}\right)_{\alpha\beta}\delta_\beta$ and $D = \sqrt{\Delta \cdot \delta}$ is the conjugate and distance of vector $\boldsymbol{\delta} = \mathbf{u}_{j,\kappa'} - \mathbf{u}_{i,\kappa}$ between atom κ' in cell j and atom κ in cell i. The short-range interaction part $\Phi^{SR}_{\kappa\alpha,\kappa'\beta}(i,j)$, which includes the short-range Pauli repulsion and all other interactions of short-range form, is obtained from the total IFC and the long-range dipole–dipole interaction.

III. Results and Discussions

(1) MLWFs of $BaMO_3$

We first examine the MLWFs of the oxygen 2*p* bands of $BaMO_3$ (M = Ti, Zr, Hf, Sn). As is shown in Figs. 1 and 2, there are three localized orbitals, which are centered on each oxygen atom of $BaMO_3$ and oriented along the M–O–M bond. According to their symmetry along the M–O–M bond, the three oxygen-centered MLWF orbitals can be separated into one MLWF orbital that is parallel to the M–O–M bond and two orbitals that are perpendicular to the M–O–M bond, and they are labeled as σ and π orbitals, respectively.[22] As can be seen from Figs. 1 and 2, The σ and π MLWF orbitals of $BaTiO_3$, $BaZrO_3$, and $BaHfO_3$ clearly illustrate the mixed ionic and covalent character of these materials. In the vicinity of the B-site and oxygen crystalline positions, the σ and π MLWF orbitals are localized and their shapes resemble the atomic orbitals of single isolated atom despite of the strong deformation by the underlying crystal potential. In between the bond-center regions, the σ and π MLWF orbitals also clearly shows the delocalized charge transfer and hybridization features between the O 2*p* orbitals and the transition metals' *d* orbitals. Comparing their charge distributions, especially those of π orbitals, we found that the valence electrons of the occupied bands are more localized on oxygen position in $BaZrO_3$ and $BaHfO_3$ than in $BaTiO_3$. This result suggests that the valence electrons of Zr and Hf have a stronger trend to be transferred to the neighbor oxygen atoms. Actually, we also found that the Bader charges of Zr and Hf are about 0.5 a.u. larger than that of Ti using first-principle calculations and charge analysis (L. Xie and J. Zhu, unpublished data), which support the large valence charge transfer of Zr and Hf in $BaZrO_3$ and $BaHfO_3$ as well. The relatively strong static charge transfer in $BaZrO_3$ and $BaHfO_3$ compared with $BaTiO_3$ can be understood. According to Slater's rule,[23] the shielding effect of the *d* electrons in Ti, Zr, and Hf are identical. That is, the effective nuclear charge Z_{eff} "seen" by the *d* electrons are the same (=3.5 a.u.) in Ti, Zr, and Hf atoms. However, the 3*d* electrons in titanium are more close to the nucleus, whereas those of Zr and Hf are on the contrary. As a result, the *d* electrons are more easily to be transferred from Zr and Hf to oxygen. In contrast with the d^0 transition metals (Ti, Zr and Hf), the 4*d* orbital of tin is fully occupied and the d^{10} electronic configuration is usually more energy favorable. Therefore, the 4*d* electrons of Sn are well localized and do not hybridize with the oxygen 2*p* electrons. This is clearly revealed in the MLWFs of $BaSnO_3$ (Figs. 1 and 2), where the oxygen 2*p* band electrons of $BaSnO_3$ are well localized on oxygen atoms and tin atom, and no sign of hybridizations between the oxygen 2*p* orbitals and the Sn 4*d* orbitals can be observed.

In conclusion, in this section, we have discussed the spatial distribution of the oxygen 2*p* bands in various $BaMO_3$ materials using MLWFs. The MLWFs clearly show delocalized charge transfer and orbital hybridizations features of the oxygen 2*p* bands in $BaTiO_3$, $BaZrO_3$ and $BaHfO_3$, whereas only localized orbitals are found in $BaSnO_3$. The calculation results also suggest a comparatively large charge transfer from the B-site atom to oxygen in $BaZrO_3$ and $BaHfO_3$. These results also demonstrate that MLWFs are useful and complementary tools for the description of electronic structures with bandstructures and density of states (DOS), which can be used to quantify the localization and orbital hybridization in real space. In what following, we will illustrate

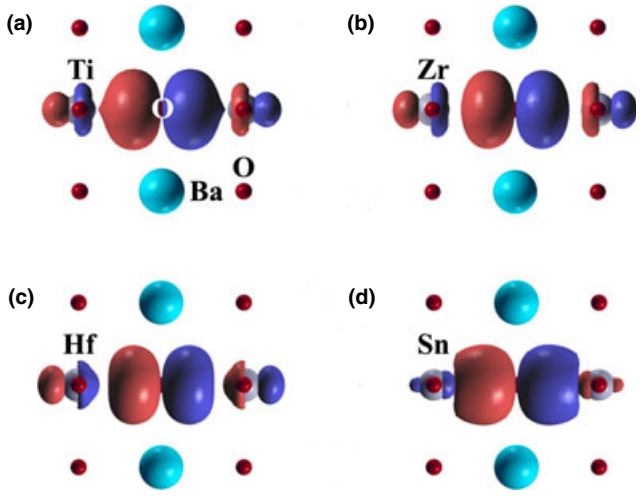

Fig. 1. Oxygen-centered σ MLWFs from the localization of the nine oxygen 2*p* bands in cubic (a) $BaTiO_3$, (b) $BaZrO_3$, (c) $BaHfO_3$, and (d) $BaSnO_3$. The orbital is oriented along the M–O–M bond and the isosurfaces of the MLWFs shown herein, are for $|W(\mathbf{r})| = 0.05$, which is about 10% of the MLWFs' maximum. The color of the isosurface refers to the sign of MLWFs: positive for dark red and negative for dark blue colors. Red balls: O sites, cyan balls: Ba sites, gray balls: B sites. In the vicinity of Ti, Zr, Hf, and O atom, the MLWF orbitals resemble the transition metals *d* orbitals and the oxygen 2*p* orbital. From the distribution of MLWFs, it can be found that the oxygen 2*p* orbitals are more localized on oxygen in $BaZrO_3$ and $BaHfO_3$, as their shapes are less affected by the *d* orbitals of Zr and Hf. The charge distribution in between the M–O bond indicate the strong orbital hybridization in $BaTiO_3$. Note that the MLWF of $BaSnO_3$ is completely different as the oxygen 2*p* orbitals are strongly distorted and the localized orbitals on Sn are of same sign, where the localized orbitals on Ti, Zr, and Hf are of different sign.

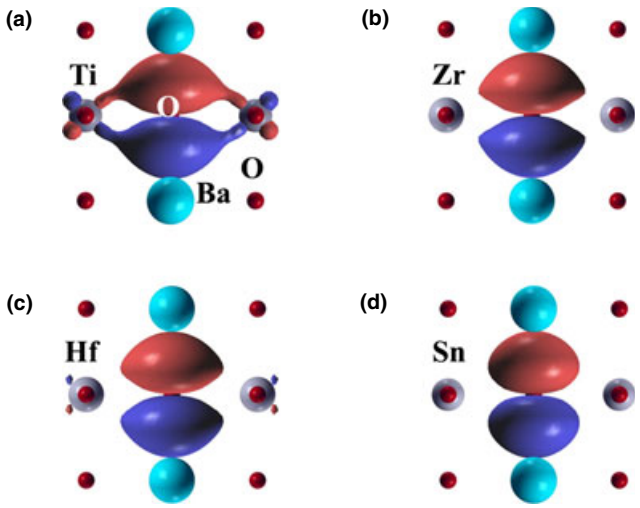

Fig. 2. Oxygen-centered π MLWFs from the localization of the nine oxygen 2*p* bands in cubic (a) $BaTiO_3$, (b) $BaZrO_3$, (c) $BaHfO_3$, and (d) $BaSnO_3$. The orbital is oriented along the M–O–M bond and the isosurfaces of MLWFs shown herein are for $|W(\mathbf{r})| = 0.05$, which is about 10% of the MLWFs' maximum. The color of the isosurface refers to the sign of MLWFs: positive for dark red and negative for dark blue colors. Red balls: O sites, cyan balls: Ba sites, gray balls: B sites. In the vicinity of Ti and O atom, the MLWF orbitals resemble the Ti 3*d* orbitals and the oxygen 2*p* orbital. The orbital hybridization between titanium and oxygen in between the Ti–O bond can also be observed directly. The MLWFs in $BaZrO_3$, $BaHfO_3$, and $BaSnO_3$ are more localized on oxygen site and they resemble the oxygen 2*p* orbitals (see text for more details).

how the dynamical effective charges are associated with the MLWFs of the oxygen 2*p* bands in these compounds.

(2) Born Effective Charge

Table I summarizes the BECs as well as the optical dielectric constants of each $BaMO_3$ compound (M = Ti, Zr, Hf, and Sn). Our calculated results for $BaTiO_3$, $BaZrO_3$, and $BaSnO_3$ are in good agreement with the literatures[7,9,24–26] given the difference in the pseudopotentials used and our choice of lattice parameters. As is shown in Table I, the BEC of Ba is almost identical (~+2.7 a.u.) in all these compounds despite of the change of local B-site chemical environments. The small effective charge anomalous (~+0.7 a.u.) suggests that the Ba atom also has some covalent character in these compounds.[22,27] For the B-site d^0 transition metals and oxygen atoms, due to the strong orbital hybridization between the transition metals' *d* and the oxygen 2*p* orbitals, their BECs are exceptionally large compared with their nominal charges (+4 a.u. and −2 a.u.). It can also be noted that the amplitude of the transition metals' BECs decreases from +7.52 a.u. to +5.84 a.u. as the increase of atomic number from Ti ($Z = 22$) to Hf ($Z = 72$). In correspondence, the amplitude of the oxygen's BECs, especially the BEC along the M–O–M bond direction, also decreases. The BEC of Sn (+4.38 a.u.) is very close to its nominal charge of +4 a.u. and therefore tin can be considered to be almost ionic in $BaSnO_3$. However, it should be noticed that the BEC $Z^*_{O_\parallel}$ of $BaSnO_3$ is still exceptionally large compared with its nominal charge (+2 a.u.), which suggests an intrinsic large anisotropy of the oxygen's dynamical effective charge in materials with perovskite structure. To inspect the microscopic origin of the anomalous contributions and identify the dynamical charge transfer, the BECs are decomposed into individual band contributions by analyzing the deformation of MLWFs under an atomic displacement, as described in Section II*(2)*. For simplicity, the BECs are decomposed by the oxygen 2*p* bands only in the following, whereasother valence bands' contributions to the BECs are not taken into account herein.

The band-by-band decomposition of the dynamical effective charges coming from the nine oxygen 2*p* bands is given in Table II. The deformation of the MLWFs under the displacement of B-site atom is shown in Figs. 3 and 4 as well. Several facts stand out from an inspection of the table. First, it is essentially the nine oxygen 2*p* bands that lead to the anomalously large BECs of the B-site atom and oxygen in these perovskite materials. For example, the O 2*p* bands contributions to the effective charges of Ti, $O_\parallel$, and $O_\perp$ are +2.96, −9.45, and −6.42, respectively. Considering the core charges of titanium (+4) and oxygen (+4) by excluding their valence electrons, the BECs of Ti, $O_\parallel$, and $O_\perp$ can be estimated as +6.96, −5.45, and −2.42, respectively. This approximation is in reasonably good agreement with the values obtained by DFPT (see Table II, for example). However, it's much complex for barium, as its dynamical effective charge also comes from the lower O 2*s*, Ba 5*s*, and Ba 5*p* bands. A full decomposition of the effective charge of barium coming from different groups of bands is given in Table III. It is interesting to point out that the sum of Ba 5*p* orbitals' and O 2*s* orbitals' contributions to the effective charge are almost identical in $BaTiO_3$, $BaZrO_3$, and $BaSnO_3$, which is an indication of the covalent feature of barium atom and explains the effective charge anomalous.

Second, it should be noted that it is the σ and π orbitals along the M–O–M bond that carry the most dynamic electronic charge Z^* with respect to the ions' displacements in the direction of M–O–M bond. Comparing the dynamical transfer of charge carried by the σ and π orbitals in these four compounds, we found that the amount of dynamical charge transfer is largest in $BaTiO_3$. Such difference can also be readily found from an inspection of their MLWFs (Figs. 3

Table I. The Born Effective Charges and Optical Dielectric Constant of $BaMO_3$ (M = Ti, Zr, Hf, and Sn)

	Z^*_{Ba}	Z^*_M	$Z^*_{O_\parallel}$	$Z^*_{O_\perp}$	ε_∞	Reference
$BaTiO_3$	+2.75	+7.16	−5.69	−2.11	–	7
	+2.74	+7.32	−5.78	−2.14	6.75	9
	+2.73	+7.52	−5.88	−2.15	6.89	Present work
$BaZrO_3$	+2.73	+6.03	−4.74	−2.01	–	24
	+2.72	+6.11	−4.81	−2.01	4.93	Present work
$BaHfO_3$	+2.72	+5.75	−4.42	−2.03	4.6	25
	+2.73	+5.84	−4.55	−2.01	4.72	Present work
$BaSnO_3$	+2.73	+4.37	−3.37	−1.87	4.89	26
	+2.74	+4.38	−3.35	−1.88	4.88	Present work

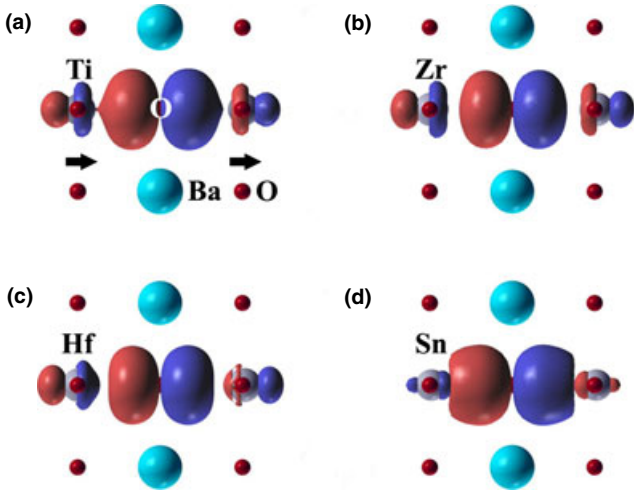

Fig. 3. Oxygen-centered σ MLWFs from the localization of the nine oxygen 2*p* bands with B-site atom displacements in (a) $BaTiO_3$, (b) $BaZrO_3$, (c) $BaHfO_3$, and (d) $BaSnO_3$. The Ti, Zr, Hf, and Sn atoms are displaced in the arrows' direction and the displacements are 1% in the fraction of lattice. The isosurfaces of the MLWFs shown herein are for $|W(\mathbf{r})| = 0.05$, which is about 10% of the MLWFs' maximum.

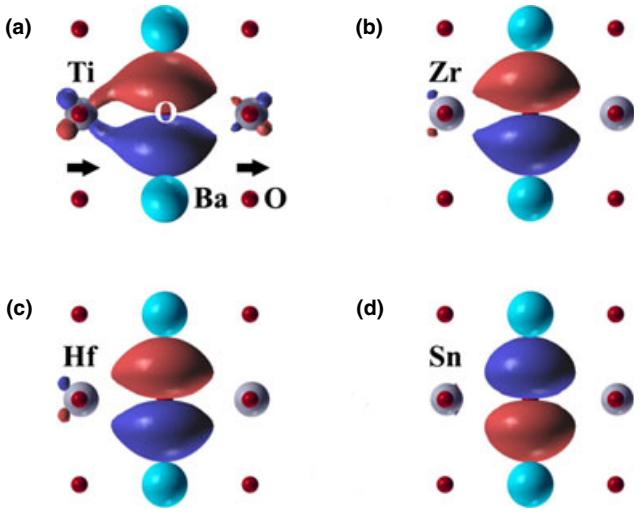

Fig. 4. Oxygen-centered π MLWFs from the localization of the nine oxygen 2*p* bands with B-site atom displacements in (a) $BaTiO_3$, (b) $BaZrO_3$, (c) $BaHfO_3$, and (d) $BaSnO_3$. The Ti, Zr, Hf, and Sn atoms are displaced in the arrows' direction and the displacements are 1% in the fraction of lattice. The isosurfaces of the MLWFs shown herein are for $|W(\mathbf{r})| = 0.05$, which is about 10% of the MLWFs' maximum. The charge transfer between the B-site Ti, Zr, Hf, and oxygen along the π orbitals can be clearly seen.

Table II. The Oxygen 2*p* Bands Decomposition of BECs (The Coordinates of Atoms are in the Fraction of Lattice with $\delta = 0.005$). The Decompositions of each Atom are Summarized in Groups and the Decomposed Effective Charge of Each Band is Given in the Horizontal Line Group

	$BaTiO_3$	$BaZrO_3$	$BaHfO_3$	$BaSnO_3$
Ba(δ,0,0)				
$(\frac{1}{2},\frac{1}{2},0)\sigma$	−0.01	−0.01	−0.01	−0.01
$(\frac{1}{2},\frac{1}{2},0)\pi$	−0.19	−0.15	−0.15	−0.13
$(\frac{1}{2},\frac{1}{2},0)\pi$	−0.19	−0.15	−0.15	−0.13
$(\frac{1}{2},0,\frac{1}{2})\sigma$	+0.11	+0.09	+0.09	+0.11
$(\frac{1}{2},0,\frac{1}{2})\pi$	+0.22	+0.16	+0.17	+0.18
$(\frac{1}{2},0,\frac{1}{2})\pi$	+0.49	+0.36	+0.38	+0.40
$(0,\frac{1}{2},\frac{1}{2})\sigma$	+0.11	+0.09	+0.09	+0.11
$(0,\frac{1}{2},\frac{1}{2})\pi$	+0.22	+0.16	+0.17	+0.18
$(0,\frac{1}{2},\frac{1}{2})\pi$	+0.49	+0.36	+0.38	+0.40
Total Z^*_{el}	+1.25	+0.91	+0.97	+1.11
Core	0	0	0	0
Total Z^*	+1.25	+0.91	+0.97	+1.11
$M(\frac{1}{2}+\delta,\frac{1}{2},\frac{1}{2})$				
$(\frac{1}{2},\frac{1}{2},0)\sigma$	+0.62	+0.49	+0.27	+0.15
$(\frac{1}{2},\frac{1}{2},0)\pi$	+1.79	+1.25	+1.14	+0.43
$(\frac{1}{2},\frac{1}{2},0)\pi$	+1.79	+1.25	+1.14	+0.43
$(\frac{1}{2},0,\frac{1}{2})\sigma$	−0.18	−0.21	−0.18	−0.26
$(\frac{1}{2},0,\frac{1}{2})\pi$	−0.16	−0.17	−0.16	−0.09
$(\frac{1}{2},0,\frac{1}{2})\pi$	−0.28	−0.24	−0.23	−0.15
$(0,\frac{1}{2},\frac{1}{2})\sigma$	−0.18	−0.21	−0.18	−0.26
$(0,\frac{1}{2},\frac{1}{2})\pi$	−0.16	−0.17	−0.16	−0.09
$(0,\frac{1}{2},\frac{1}{2})\pi$	−0.28	−0.24	−0.23	−0.15
Total Z^*_{el}	+2.96	+1.75	+1.41	+0.01
Core	+4	+4	+4	+4
Total Z^*	+6.96	+5.75	+5.41	+4.01
$O_{\parallel}(\delta,\frac{1}{2},\frac{1}{2})$				
$(\frac{1}{2},\frac{1}{2},0)\sigma$	−2.65	−2.48	−2.25	−1.53
$(\frac{1}{2},\frac{1}{2},0)\pi$	−3.11	−2.76	−2.68	−2.18
$(\frac{1}{2},\frac{1}{2},0)\pi$	−3.11	−2.76	−2.68	−2.18
$(\frac{1}{2},0,\frac{1}{2})\sigma$	−0.10	−0.04	−0.06	−0.19
$(\frac{1}{2},0,\frac{1}{2})\pi$	−0.01	−0.02	−0.02	−0.02
$(\frac{1}{2},0,\frac{1}{2})\pi$	−0.18	−0.18	−0.18	−0.17
$(0,\frac{1}{2},\frac{1}{2})\sigma$	−0.10	−0.04	−0.06	−0.19
$(0,\frac{1}{2},\frac{1}{2})\pi$	−0.01	−0.02	−0.02	−0.02
$(0,\frac{1}{2},\frac{1}{2})\pi$	−0.18	−0.18	−0.18	−0.17
Total Z^*_{el}	−9.45	−8.48	−8.13	−6.65
Core	+4	+4	+4	+4
Total Z^*	−5.45	−4.48	−4.13	−2.65
$O_{\perp}(\frac{1}{2}+\delta,\frac{1}{2},0)$				
$(\frac{1}{2},\frac{1}{2},0)\sigma$	−1.86	−1.83	−1.87	−1.69
$(\frac{1}{2},\frac{1}{2},0)\pi$	−1.88	−1.86	−1.84	−1.93
$(\frac{1}{2},\frac{1}{2},0)\pi$	−2.28	−2.17	−2.19	−2.29
$(\frac{1}{2},0,\frac{1}{2})\sigma$	+0.03	+0.01	+0.02	+0.03
$(\frac{1}{2},0,\frac{1}{2})\pi$	+0.02	+0.02	+0.02	+0.02
$(\frac{1}{2},0,\frac{1}{2})\pi$	+0.04	+0.04	+0.04	+0.03
$(0,\frac{1}{2},\frac{1}{2})\sigma$	+0.02	+0.00	−0.01	−0.15
$(0,\frac{1}{2},\frac{1}{2})\pi$	+0.00	−0.02	−0.02	−0.01
$(0,\frac{1}{2},\frac{1}{2})\pi$	−0.51	−0.33	−0.31	−0.11
Total Z^*_{el}	−6.42	−6.14	−6.16	−6.10
Core	+4	+4	+4	+4
Total Z^*	−2.42	−2.14	−2.16	−2.10

and 4), where sizable charges "flow" from oxygen to titanium along the Ti–O–Ti chain can be observed. For Zr and Hf, as can be seen in Figs. 1[(b),(c)] and 2[(b),(c)], their valence electrons are more delocalized and have already been partially transferred to oxygen atoms. As a result, their mobile charges that can "flow" between the B-site ion and oxygen are less than those in $BaTiO_3$. This dynamical charge transfer effect is even less pronounced for the *d*-state full occupied tin because orbital hybridizations are required for the charge transfer to take place.[22] Besides, the dynamical charge transfers, which induce the large effective charge, it should also be noted that there is a charge compensation effect of the B-site atoms. The effective charges induced by local 2*p* σ and π orbitals are partially canceled by other 2*p* σ and π orbitals. For instance, the dynamic charges of the three oxygen 2*p* σ and π orbitals centered at $(\frac{1}{2},\frac{1}{2},0)$ are compensated

Table III. The Band-by-Band Decomposition of the BEC of Barium in $BaMO_3$ (M = Ti, Zr, Hf, and Sn) (The Barium Atom is Displaced in the Fraction of Lattice with $\delta = 0.005$). The Decomposition of Each Band Group is Summarized and the Decomposed Effective Charge of Each Band is Given in the Horizontal Line Group

	$BaTiO_3$	$BaZrO_3$	$BaHfO_3$	$BaSnO_3$
Ba 5*s*	−2.08	−2.02	−2.04	−2.06
Ba 5*p*	−7.13	−6.73	−7.81	−6.86
(0,0,0)	−2.43	−2.29	−2.69	−2.32
(0,0,0)	−2.35	−2.22	−2.56	−2.27
(0,0,0)	−2.35	−2.22	−2.56	−2.27
M *s*	+0.01	+0.01	+0.01	–
M *p*	+0.02	+0.05	+0.05	–
$(\frac{1}{2},\frac{1}{2},\frac{1}{2})$	+0.00	+0.01	+0.01	–
$(\frac{1}{2},\frac{1}{2},\frac{1}{2})$	+0.01	+0.02	+0.02	–
$(\frac{1}{2},\frac{1}{2},\frac{1}{2})$	+0.01	+0.02	+0.02	–
M *d*	–	–	–	+0.10
$(\frac{1}{2},\frac{1}{2},\frac{1}{2})$	–	–	–	+0.03
$(\frac{1}{2},\frac{1}{2},\frac{1}{2})$	–	–	–	+0.02
$(\frac{1}{2},\frac{1}{2},\frac{1}{2})$	–	–	–	+0.02
$(\frac{1}{2},\frac{1}{2},\frac{1}{2})$	–	–	–	+0.02
$(\frac{1}{2},\frac{1}{2},\frac{1}{2})$	–	–	–	+0.01
M *f*	–	–	+0.98	–
$(\frac{1}{2},\frac{1}{2},\frac{1}{2})$	–	–	+0.22	–
$(\frac{1}{2},\frac{1}{2},\frac{1}{2})$	–	–	+0.04	–
$(\frac{1}{2},\frac{1}{2},\frac{1}{2})$	–	–	+0.04	–
$(\frac{1}{2},\frac{1}{2},\frac{1}{2})$	–	–	+0.05	–
$(\frac{1}{2},\frac{1}{2},\frac{1}{2})$	–	–	+0.11	–
$(\frac{1}{2},\frac{1}{2},\frac{1}{2})$	–	–	+0.26	–
$(\frac{1}{2},\frac{1}{2},\frac{1}{2})$	–	–	+0.26	–
O 2*s*	+0.60	+0.46	+0.46	+0.44
$(\frac{1}{2},\frac{1}{2},0)$	–0.10	–0.08	–0.08	–0.10
$(\frac{1}{2},0,\frac{1}{2})$	+0.35	+0.27	+0.27	+0.27
$(0,\frac{1}{2},\frac{1}{2})$	+0.35	+0.27	+0.27	+0.27
Total Z^*_{el}	–7.33	–7.32	–7.38	–7.27
Core	10	10	10	10
Total Z^*_{Ba}	+2.67	+2.68	+2.62	+2.73

by the orbitals centered at $(\frac{1}{2},0,\frac{1}{2})$ and $(0,\frac{1}{2},\frac{1}{2})$, when the B-site atom is off-center displaced from $(\frac{1}{2},\frac{1}{2},\frac{1}{2})$ to $(\frac{1}{2}+\delta,\frac{1}{2},\frac{1}{2})$. This mutual compensation effect is most significant for Sn atom and leads to an almost zero contribution of the valence oxygen 2*p* bands. As a result, the anomalous charge contribution due to the dynamic charge transfer between tin and oxygen is very small and the effective charge of tin is close to its nominal charge +4 a.u.

It is interesting to point out that the effective charge may also be related to the materials' band-gaps since a lower charge-transfer band-gap can be more effective for the dynamic charge transfer if other material conditions are fixed the same. From our theoretical calculations, the band-gaps for $BaTiO_3$, $BaZrO_3$, and $BaHfO_3$ are 1.92 eV, 3.36 eV, and 3.75 eV, respectively. This trend reasonably reflects the difference of the dynamic charge transfer in these materials.

(3) Interatomic Force Constants

In the previous sections, the microscopic origin of anomalous effective charges in compounds $BaTiO_3$, $BaZrO_3$, and $BaHfO_3$, and $BaSnO_3$ is discussed by analyzing their valence charge distribution and dynamical effective charges. The calculation results clearly show that the anomalous large effective charge in $BaTiO_3$, $BaZrO_3$, and $BaHfO_3$ majorly originates from the dynamic transfer of charge between the transition metal *d* orbitals and oxygen 2*p* orbitals. In this section, a complementary instructive picture of the atom interactions, especially the long-range dipole–dipole interactions associated with the dynamical effective charges in response to the motion of atoms is provided by direct examinations of the real-space interatomic force constants.

The IFCs are generated in the approach as described in Section II and the results for $BaTiO_3$, $BaZrO_3$, and $BaHfO_3$ and $BaSnO_3$ are given in Tables IV and V. For convenience, the atoms are labeled according to Ref. 28 and their schematic view is illustrated in Fig. 5. First, we examine the "self-force constant" term (see Table IV), which describes the force exert on a single atom, which is displaced from its position, whereas other atoms are kept fixed. The self-force constants are positive for all atoms in these four compounds, which means that single atomic displacement is not energy stable and will not give rise to the structure instabilities. Instead, only cooperative atomic displacements can reduce the total energy and lead to the ferroelectricity. It should be

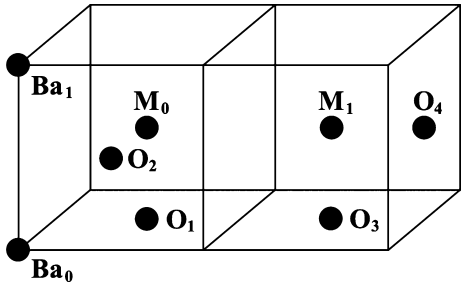

Fig. 5. Schematic view of the atoms labeled in Table V.

Table IV. Self-Force Constants (eV/Å^2) on the Different Atoms of $BaMO_3$ (M = Ti, Zr, Hf, and Sn)

Atom	Direction	$BaTiO_3$	$BaZrO_3$	$BaHfO_3$	$BaSnO_3$
Ba	$x = y = z$	+8.1300	+5.2103	+5.6329	+6.6857
M	$x = y = z$	+14.3766	+20.6001	+21.5745	+24.5780
O	$x = y$	+6.7529	+3.9122	+4.5349	+3.8430
	z	+12.2630	+19.6563	+20.6409	+21.8975

Table V. Selected Longitudinal (∥), Transverse (⊥), Interatomic Force Constants (eV/Å^2) Between Different Pairs of Atoms. The Dipole–Dipole (DD) and Short-Range (SR) Force are Separated Following Section II

		$BaTiO_3$			$BaZrO_3$			$BaHfO_3$			$BaSnO_3$		
Atom		Total	DD	SR	Total	DD	SR	Total	DD	SR	Total	DD	SR
M_0–O_1	(∥)	1.3265	+23.1026	−21.7761	−3.3109	+18.6527	−21.9636	−3.5357	+17.8859	−21.4215	−6.9346	+9.9198	−16.8544
	(⊥)	−1.9422	−4.2177	+2.2755	−1.6150	−3.8955	+2.2805	−1.8232	−3.9498	+2.1266	−1.2939	−2.7884	+1.4945
M_0–M_1	(∥)	−7.5495	−3.6893	−3.8601	−6.1428	−2.9589	−3.1839	−5.9564	−2.8691	−3.0873	−3.2239	−1.6209	−1.6030
	(⊥)	+0.5975	+1.8447	−1.2472	+0.5602	+1.4794	−0.9192	+0.5526	+1.4346	−0.8820	+0.1826	+0.8105	−0.6279
M_0–O_4	(∥)	+2.9145	+0.8557	+2.0588	+2.3833	+0.6908	+1.6924	+2.3256	+0.6624	+1.6632	+0.5828	+0.3674	+0.2154
	(⊥)	−0.1611	−0.1562	−0.0049	−0.1382	−0.1443	+0.0060	−0.1441	−0.1463	+0.0021	−0.1475	−0.1033	−0.0442
M_0–Ba_0	(∥)	−2.8741	−2.0633	−0.8109	−2.7809	−2.0297	−0.7512	−2.8396	−2.0641	−0.7755	−2.6101	−1.5602	−1.0500
	(⊥)	+1.1490	+1.0316	+0.1174	+1.1074	+1.0148	+0.0926	+1.1261	+1.0320	+0.0941	+0.9712	+0.7801	+0.1911
	(xx)	−0.1920	+0.0000	−0.1920	−0.1887	+0.0000	−0.1887	−0.1958	+0.0000	−0.1958	−0.2226	+0.0000	−0.2226
Ba_0–O_1	(∥)	−0.1111	+1.0833	−1.1945	+0.6082	+1.2273	−0.6191	+0.5397	+1.3051	−0.7653	+0.2164	+1.2327	−1.0163
	(zz)	−0.9765	−1.4835	+0.5070	−0.9423	−1.4691	+0.5268	−0.9422	−1.4774	+0.5353	−0.8305	−1.0963	+0.2658
Ba_0–Ba_1	(∥)	−1.1504	−0.4868	−0.6636	−0.9936	−0.5874	−0.4062	−1.0395	−0.6265	−0.4131	−1.1349	−0.6335	−0.5013
	(⊥)	+0.3458	+0.2434	+0.1024	+0.3613	+0.2937	+0.0676	+0.3797	+0.3132	+0.0665	+0.3765	+0.3168	+0.0597

noted herein that the self-force constants of Ti and O(z) in $BaTiO_3$ are 6–10 eV/Å^2 smaller than those in $BaZrO_3$, $BaHfO_3$, and $BaSnO_3$. Therefore, the potential well at B and oxygen sites of $BaTiO_3$ is relatively shallow and titanium atom can move more easily in the oxygen octahedra than Zr, Hf, and Sn.

Next, we discuss the IFCs between different atoms if we consider the case where only two-first nearest-neighbor barium, B-site atoms, and B-site/O atoms are allowed to displace. In addition to the total IFCs, the IFC tensor is also decomposed into individual long-range dipole–dipole and short-range interactions following the approach described in Section II. From an inspection of Table V, it can be readily found that the interactions between barium and barium, and barium and neighbor B-site atoms in these four compounds are quite similar and their energy differences are very small except for the Ba_0–O_1 interactions. The interaction between barium and the nearest oxygen is repulsive in $BaTiO_3$ and attractive in other three compounds. From an investigation of the Ba_0–O_1 short-range interaction, we find that the amplitude of the short-range interaction increases as the decrease of the lattice parameter. As a result, the attractive Ba_0–O_1 dipole–dipole interaction in $BaTiO_3$ is canceled by the short-range Pauli repulsion, and the total Ba_0–O_1 interatomic interaction is repulsive. For B-site atoms, the longitudinal components of the M_0–M_1 interatomic force increase in the order of Ti_0–$Ti_1(\|)$, Zr_0–$Zr_1(\|)$, Hf_0–$Hf_1(\|)$, and Sn_0–$Sn_1(\|)$. In $BaTiO_3$, the contribution from cooperative Ti_0–$Ti_1(\|)$ displacements is enhanced by both the dipole–dipole and short-range interactions, which are sufficient to compensate the stabilizing self-force constant (Table IV) and induce the instable Ti–O–Ti chain-like structure.[29] For $BaZrO_3$, $BaHfO_3$, and $BaSnO_3$, the potential well at B-site is much steeper, so that the B-site cations' cooperative displacements can only partially compensate the stabilizing self-force constant. The negative sign of the longitudinal force constant of M_0–M_1 indicates that the ferroelectricity is favored over anti-ferroelectricity. This can be readily understood from the long-range dipole–dipole interaction and short-range interaction between M_0–M_1 (Eq. 5). As M_0 and M_1 have identical BEC, their long-range dipole–dipole interactions in the longitudinal direction are always negative. That is, the long-range dipole–dipole interactions between M_0 and M_1 will always favor the long-range ferroelectric ordering. For the short-range interactions between M_0–M_1 in the longitudinal direction, they are all negative and also in favor of the ferroelectric ordering. However, it should be pointed out that if the short-range interaction between M_0–M_1 is positive and large enough to compensate the negative long-range dipole–dipole interaction, it is possible for the anti-ferroelectricity ordering to be formed.

In addition to the destabilizing Ti_0–$Ti_1(\|)$ interaction, the positive Ti_0–$O_1(\|)$ interaction, although relatively small, make another important contribution to the ferroelectric instability, where the displacement of O_1 atom against the Ti_0 atom along the Ti–O chain direction is energy favorable. It is worth pointing out that the Ti_0–$O_1(\|)$ interatomic force is the result of a delicate balance between the attractive dipole–dipole and the repulsive short-range interactions. According to Eq. (8), the long-range dipole–dipole interaction between the B-site atom and oxygen is proportional to the B-site atom's dynamical effective charge. As a result, the long-range dipole–dipole interaction between titanium and oxygen is sufficient to compensate the repulsive short-range interaction and give rise to the instable polar Ti_0–$O_1(\|)$ displacements. As a comparison, the interactions between Zr_0–$O_1(\|)$, Hf_0–$O_1(\|)$, and Sn_0–$O_1(\|)$ are all repulsive, asthe effective charges of Zr, Hf, and Sn are comparatively smaller and the attractive dipole–dipole interaction between B-site cation and the nearest oxygen is insufficient to completely compensate their short-range repulsive interaction. Therefore the Zr, Hf or Sn cations do not move against oxygen atoms, but would rather with them in the same direction along the M–O chain.

(4) Discussions

In Sections III*(1)* and *(2)*, we have discussed the charge distribution of the oxygen 2p bands and its dynamical response to the motion of atoms through the MLWFs. First, we remark that the oxygen 2p bands strongly depend on the choice of B-site atom. For the d-state transition metals, their outer d orbitals strongly hybridize with the oxygen 2p orbitals and form a σ and two π orbitals along the M–O–M bond direction. These orbitals carry the most mobilized charge and their dynamical response to the motion of atoms lead to the anomalous large BECs in these compounds. For the d-state full occupied tin metal, its d orbitals are firmly localized on atom position and do not hybridize with the oxygen 2p orbitals. As a consequence, the d orbitals of tin will move rigidly with respect to the motion of tin and its effective charge is very close to its nominal ionic charge. This essential difference between the orbital hybridizations of d-state transition metal and d-state full occupied metal provides the covalent-ionic picture and pure ionic picture of these perovskite compounds, respectively. Next, we remark that the oxygen 2p bands of $BaZrO_3$ and $BaHfO_3$ are more localized on oxygen than those of $BaTiO_3$ (see Figs. 1 and 2 for example). This result originates in the relative electronegativity of the B-site atoms and oxygen. The charges of Zr and Hf are more easily to be transferred to oxygen than those of Ti. Therefore, $BaZrO_3$ and $BaHfO_3$ are more ionic than $BaTiO_3$ and the effective charges of Zr and Hf are relatively close to their nominal value. It should also be remarked that the dynamical effective charges of barium is not very sensitive to the B-site atom. This fact provides another example of the covalent character of the bonding between Ba and O, which results in the delicate charge compensation between Ba 5p and O 2s orbitals (see Table III).

In Section III*(3)*, we have discussed the self-force constants as well as the IFCs of $BaTiO_3$, $BaZrO_3$, $BaHfO_3$, and $BaSnO_3$. First, we remark the fact that the self-force constants of B-site atoms and oxygen are all positive in these materials. In terms of lattice dynamics, the self-force constant can be written as a sum over IFCs and it can be easily verified that the positive self-force constants would correspond to the potential well with only one single local minimum at the origin. It is worth pointing out that even for $BaTiO_3$ this single potential well model is still valid, despite of the relatively small self-force constants. On the contrary, experiments using X-ray diffraction,[29] X-ray Absorption Fine Structure,[30] and first-principle calculations[3] suggested an eight-site order-disorder model, of which the potential well of titanium has eight equivalent local minima along {111} directions, instead of one single local minimum. As we've discussed above, the stable Ti self-force constant can nearly be compensated by the destabilizing effect from the Ti_0–$Ti_1(\|)$ interactions. As a consequence, the stable displacement of single titanium atom along <111> directions can be destabilized by the cooperative interactions of neighboring Ti atoms. The net effect of the competition between the stable self-force constant and the instable Ti–Ti interactions is to give rise to the correlated displacements of titanium atoms along eight equivalent {111} directions and leads to the experimentally observed off-center displacements along {111} directions.

Next, we remark that the M–O interactions are repulsive in $BaZrO_3$, $BaHfO_3$, and $BaSnO_3$, and attractive in $BaTiO_3$. The SR force contribution to the M–O interaction in $BaTiO_3$, $BaZrO_3$, and $BaHfO_3$ are very similar, so that the difference arises from the DD force contribution. In $BaTiO_3$, the DD force is dominative against the SR force as a result of the larger BECs of titanium and oxygen (see Table I) and the net effect is to promote the instable Ti–O displacements and ferroelectricity. In $BaZrO_3$, $BaHfO_3$, and $BaSnO_3$, even

though the DD force contribution is partly increased by the smaller optical dielectric constant ε_∞ (see Table I), it is still not large enough to compensate the SR force contribution and therefore the ferroelectric Zr–O, Hf–O, and Sn–O distortions are suppressed. This again provides the example of the very delicate nature of the competition between SR and DD forces in these perovskites.

The above analysis of dynamical oxygen 2*p* bands and IFC in real space together provides an insightful picture of the driving mechanism of ferroelectricity in these materials. A systematic comparison between $BaTiO_3$, $BaZrO_3$, $BaHfO_3$, and $BaSnO_3$ clearly reveals the role of charge transfer between B-site atom and oxygen. In response to the motion of B-site atoms and oxygen atoms, the charges are transferred and redistributed via oxygen 2*p* orbitals. As discussed above, this dynamic charge transfer is closely related to the BEC and therefore the long-range DD force constants. In $BaTiO_3$, this charge transfer effect is so strong that the long-range DD interactions of Ti–Ti and Ti–O are nearly enough to promote the ferroelectric instability. In $BaZrO_3$, $BaHfO_3$, and $BaSnO_3$, the long-range M–M and M–O DD interactions are relatively small in consequence of the smaller charge transfer of oxygen 2*p* bands. Therefore, the materials remain stable against the ferroelectric M–M and M–O distortions.

IV. Conclusions

In thisstudy, we have discussed in detail the electronic structure, dynamical effective charge, and real-space IFCs of cubic $BaTiO_3$, $BaZrO_3$, $BaHfO_3$ and $BaSnO_3$. The electronic structure as well as the dynamical effective charge of $BaMO_3$ with M = Ti, Zr, Hf, and Sn are understood by considering their real-space MLWFs. In $BaTiO_3$, $BaZrO_3$, and $BaHfO_3$ where the B-site atoms are d^0 transition metals, their outer *d*-state electrons strongly hybridize with the oxygen 2*p* orbital and forming a σ and two π orbitals along the M–O–M bonding direction. Further analysis of the electronic structures by a band-by-band decomposition of the BECs clearly reveals that these hybridized orbitals carry the most dynamical effective charge and plays an important role in the charge transfer between B-site atoms and oxygen. In $BaSnO_3$, the d^{10} electronic structure of tin is more energy favorable and there is no hybridization between the *d*-state electrons of tin with oxygen 2*p* orbitals. As a consequence, the dynamic charges are firmly localized upon tin atoms and its BEC is close to its nominal +4 charge value. Our calculation results demonstrated that the MLWF description of electronic structures is a useful complementary tool over bandstructures and DOS in describing the localization and orbital hybridization of valence electrons in real space.

On the basis of the electronic structure investigations, we also carried out systematically studies of the IFCs. We found that the hybridized orbitals are also a crucial factor in modifying the interaction between the B-site atom and oxygen. In $BaTiO_3$, the long-range DD force associated with the large BEC are strong enough to compensate the stable self-force constants, giving rise to the unstable Ti_0–Ti_1 (||) and Ti–O interactions and the ferroelectric instability. As the decrease of dynamic charge transfer and BECs, the long-range DD interactions along the M–O bonds are reduced and the unstable ferroelectric distortions of Zr–O, Hf–O, and Sn–O are all suppressed. This calculation result again confirms the importance of orbital hybridization in the promotion of ferroelectric instability in materials with perovskite, and is crucial for understanding the origin of ferroelectric property in these materials.

Acknowledgments

This study is financially supported by National 973 Project of China and Chinese National Nature Science Foundation. This study made use of the resources of the Beijing National Center for Electron Microscopy. The authors thank Professor Chunlei Wang for helpful discussions.

References

[1]K. Uchino, *Piezoelectric Actuators and Ultrasonic Motors*. Kluwer Academic, Boston, (1996).
[2]K. Abe and S. Komatsu, "Ferroelectric Properties in Epitaxially Grown $Ba_xSr_{1-x}TiO_3$ Thin Films," *J. Appl. Phys.*, **77** [12] 6461, 5pp (1995).
[3]R. E. Cohen, "Origin of Ferroelectricity in Perovskite Oxides," *Nature*, **358**, 136–8 (1992).
[4]J. A. Kittl, K. Opsomera, M. Popovicia, N. Menoua, B. Kaczera, X. P. Wanga, C. Adelmanna, M. A. Pawlaka, K. Tomidaa, A. Rothschilda, B. Govoreanua, R. Degraevea, M. Schaekersa, M. Zahida, A. Delabiea, J. Meersschauta, W. Polspoela, S. Climaa, G. Pourtoisa, W. Knaepenb, C. Detavernierb, V. V. Afanas'evc, T. Blombergd, D. Pierreuxe, J. Swertse, P. Fischere, J. W. Maese, D. Mangerf, W. Vandervorsta, T. Conarda, A. Franqueta, P. Faviaa, H. Bendera, B. Brijsa, S. Van Elshochta, M. Jurczaka, J. Van Houdta, and D. J. Woutersa, "High-k Dielectrics for Future Generation Memory Devices," *Microelectron. Eng.*, **86** [7–9] 1789–95 (2009).
[5]R. D. King-Smith and D. Vanderbilt, "Theory of Polarization of Crystalline Solids," *Phys. Rev. B*, **47**, 1651–4 (1993).
[6]R. Resta, "Macroscopic Polarization in Crystalline Dielectrics: The Geometric Phase Approach," *Rev Mod Phys*, **66**, 899–915 (1994).
[7]W. Zhong, R. D. King-Smith, and D. Vanderbilt, "Giant LO-TO Splittings in Perovskite Ferroelectrics," *Phys. Rev. Lett.*, **72**, 3618–21 (1994).
[8]U. V. Waghmare, N. A. Spaldin, H. C. Kandpal, and R. Seshadri, "First-Principles Indicators of Metallicity and Cation off-Centricity in the IV-VI Rocksalt Chalcogenides of Divalent Ge, Sn, and Pb," *Phys. Rev. B*, **67**, 125111 (2003).
[9]Ph. Ghosez, X. Gonze, and J.-P. Michenaud, "AB Initio Phonon Dispersion Curves and Interatomic Force Constants of Barium Titanate," *Ferroelectrics*, **206** [1] 205–17 (1998).
[10]G. Kresse and J. Furthmüller, "Efficient Iterative Schemes for ab Initio Total-Energy Calculations Using a Plane-Wave Basis set," *Phys. Rev. B*, **54**, 11169 (1996).
[11]G. Kresse and D. Joubert, "From Ultrasoft Pseudopotentials to the Projector Augmented-Wave Method," *Phys. Rev. B*, **59**, 1758 (1999).
[12]J. P. Perdew and A. Zunger, "Self-Interaction Correction to Density-Functional Approximations for Many-Electron Systems," *Phys. Rev. B*, **23**, 5048 (1981).
[13]H. J. Monkhorst and J. D. Pack, "Special Points for Brillouin-Zone Integrations," *Phys. Rev. B*, **13**, 5188 (1976).
[14]S. Baroni, P. Giannozzi, and A. Testa, "Green's-Function Approach to Linear Response in Solids," *Phys. Rev. Lett.*, **58**, 1861 (1987).
[15]X. Gonze, D. C. Allan, and M. P. Teter, "Dielectric Tensor, Effective Charges, and Phonons in α-Quartz by Variational Density-Functional Perturbation Theory," *Phys. Rev. Lett.*, **68**, 3603 (1992).
[16]F. Freimuth, Y. Mokrousov, D. Wortmann, S. Heinze, and S. Blügel, "Maximally Localized Wannier Functions Within the FLAPW Formalism," *Phys. Rev. B*, **78**, 035120 (2008).
[17]A. A. Mostofi, J. R. Yates, Y.-S. Lee, I. Souza, D. Vanderbilt, and M. Marzari, "Wannier90: A Tool for Obtaining Maximally-Localised Wannier Functions," *Comput. Phys. Commun.*, **178** [9] 685–99 (2008).
[18]N. Marzari and D. Vanderbilt, "Maximally Localized Generalized Wannier Functions for Composite Energy Bands," *Phys. Rev. B*, **56**, 12847 (1997).
[19]J. Bhattacharjee and U. V. Waghmare, "Localized Orbital Description of Electronic Structures of Extended Periodic Metals, Insulators, and Confined Systems: Density Functional Theory Calculations," *Phys. Rev. B*, **73**, 121102 (2006).
[20]X. Gonze, J.-C. Charlier, D. C. Allan, and M. P. Teter, "Interatomic Force Constants From First Principles: The Case of α-Quartz," *Phys. Rev. B*, **50**, 13035 (1994).
[21]Ph. Ghosez, X. Gonze, and J.-P. Michenaud, "Lattice Dynamics and Ferroelectric Instability of Barium Titanate," *Ferroelectrics*, **194** [1] 39–54 (1997).
[22]N. Marzari and D. Vanderbilt, "Maximally-Localized Wannier Functions in Perovskites: Cubic $BaTiO_3$," arXiv:cond-mat/9802210v1.
[23]J. C. Slater, "Atomic Shielding Constants," *Phys. Rev.*, **36** [1] 57–64 (1930).
[24]Ph. Ghosez, J.-P. Michenaud, and X. Gonze, "Dynamical Atomic Charges: The Case of ABO_3 Compounds," *Phys. Rev. B*, **58**, 6224–40 (1998).
[25]R. Vali, "Lattice Dynamics and Electronic Properties of the Scintillator Host Material: Barium Hafnate," *Sol. State Commun.*, **147**, 1–2 (2008).
[26]E. Bévillon, A. Chesnaud, Y. Z. Wang, G. Dezanneau, and G. Geneste, "Theoretical and Experimental Study of the Structural, Dynamical and Dielectric Properties of Perovskite $BaSnO_3$," *J. Phys.: Condens. Matter*, **20** [14] 145217, 6pp (2008).
[27]Ph. Ghosez, X. Gonze, Ph. Lambin, and J.-P. Michenaud, "Born Effective Charges of Barium Titanate: Band-by-Band Decomposition and Sensitivity to Structural Features," *Phys. Rev. B*, **51**, 6765–8 (1995).
[28]Ph. Ghosez, E. Cockayne, U. V. Waghmare, and K. M. Rabe, "Lattice Dynamics of $BaTiO_3$, $PbTiO_3$, and $PbZrO_3$: A Comparative First-Principles Study," *Phys. Rev. B*, **60**, 836–43 (1999).
[29]R. Comes, M. Lambert, and A. Guinier, "The Chain Structure of $BaTiO_3$ and $KNbO_3$," *Sol. State Commun.*, **6** [10] 715–9 (1968).
[30]B. Ravel, E. A. Stern, R. I. Vedrinskii, and V. Kraizman, "Local Structure and the Phase Transitions of $BaTiO_3$," *Ferroelectrics*, **206** [1] 407–30 (1998). □